Transport properties of single TiO2 nanotubes

Markus Stiller, José Barzola-Quiquia, Israel Lorite, Pablo Esquinazi, Robin Kirchgeorg, Sergiu P. Albu, and Patrik Schmuki

---

Articles you may be interested in

Improved visible solar absorber based on TiO2 nanotube film by surface-loading of plasmonic Au nanoparticles
J. Appl. Phys. **114**, 063510 (2013); 10.1063/1.4818441

Erratum: "Investigation of electrical transport in anodized single TiO2 nanotubes" [Appl. Phys. Lett. 102, 043105 (2013)]
Appl. Phys. Lett. **103**, 039901 (2013); 10.1063/1.4815940

Electrical property measurements of Cr-N codoped TiO2 epitaxial thin films grown by pulsed laser deposition
Appl. Phys. Lett. **102**, 172108 (2013); 10.1063/1.4804240

Investigation of electrical transport in anodized single TiO2 nanotubes
Appl. Phys. Lett. **102**, 043105 (2013); 10.1063/1.4789763

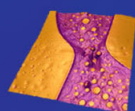Transport properties in single-crystalline rutile TiO2 nanorods
Appl. Phys. Lett. **99**, 222107 (2011); 10.1063/1.3665635
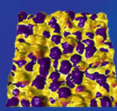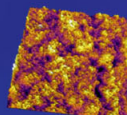
Transport properties of single TiO$_2$ nanotubes

Markus Stiller,[1] José Barzola-Quiquia,[1] Israel Lorite,[1] Pablo Esquinazi,[1] Robin Kirchgeorg,[2] Sergiu P. Albu,[2] and Patrik Schmuki[2,3]

[1]*Division of Superconductivity and Magnetism, Institute for Experimental Physics II, University of Leipzig, D-04103 Leipzig, Germany*
[2]*Chair for Surface Science and Corrosion Department Material Science and Engineering, University of Erlangen, D-91058 Erlangen, Germany*
[3]*Department of Chemistry, King Abdulaziz University, Jeddah, Saudi Arabia*

We investigated the electric transport properties of single TiO$_2$ nanotubes separated from an anodic titania nanotube array. The temperature dependence of the resistance measured with the conventional four point method of all investigated samples show a Mott variable range hopping behavior. The results obtained with two contacts indicate the existence of a potential barrier between the Cr/Au contacts and samples surfaces, which influence is clearly observable at temperatures <150 K. Impedance spectroscopy in the frequency range of 40 Hz to 1 MHz carried out at room temperature indicates that the electronic transport of these polycrystalline tubes is dominated by the grain cores. © 2013 AIP Publishing LLC. [http://dx.doi.org/10.1063/1.4826640]

In the last decade, titanium dioxide nanotube arrays, formed by self-organizing anodization, have attracted considerable attention. Mainly these 1D structures are expected to replace titanium dioxide nanostructured particulate electrodes in catalysis,[1] photocatalysis,[2] dye-synthesized solar cells,[3] gas sensors,[4] or batteries,[5] due to improved electron transfer properties. Electronic, chemical, and ionic properties of TiO$_2$ depend considerably on the specific phase of TiO$_2$.[6,7] Rutile and anatase are the most used phases in many applications of TiO$_2$ based on charge transfer reactions (solar cells, photocatalysis).[8–12] Nevertheless, the general mechanism for electron transport, particularly in nanostructures, is not well studied and understood. The transport properties can be strongly influenced by the scattering as well as through the possible increase of the carrier density at the grain boundaries, namely, in polycrystalline nanotube arrays.[13] Additionally, the sample surfaces containing intergranular boundaries may play an extra role in the conductivity. In the present work, we investigated the conductivity of single TiO$_2$ nanotubes separated from anodic TiO$_2$ nanotube arrays. The relatively simple way to produce such self-organized TiO$_2$ nanotubes on Ti substrates makes this approach cheap and efficient compared to other fabrication techniques. These TiO$_2$ tubes are usually amorphous after growing but can be converted to anatase by annealing at temperatures (T) higher than 300 °C.[14,15] After annealing, the nanotubes are polycrystalline with an average grain size of 10 to 50 nm.[16,17] We have used impedance spectroscopy in order to discern between the mechanisms of conduction given by the possible electron pathways in the sample.[18] To characterize the contact resistance we have also studied the current-voltage (I–V) characteristics using two points measurements as recently reported for single TiO$_2$ nanotubes.[19]

Prior to anodization the titanium foils (Advent Ltd., 99,6%, 0.1 mm) were cleaned by sonicating them in acetone, ethanol, and deionized (DI) water and were then dried in a nitrogen stream. The TiO$_2$ nanotubes were grown by anodization using a potentiostat (Jaissle IMP 88 PC) in a three electrode setup, where a platinum sheet acts as counter, a platinum wire as reference, and the Ti foil as working electrode. The anodization was carried out at room temperature in an ethylene glycol (Sigma Aldrich 99.5%) 0.15 mol/l ammonium fluoride electrolyte (Sigma Aldrich) with 1 M H$_2$O at 60 V for 10 h. After anodization, the grown layers were immersed in ethanol for 1 h and dried in a nitrogen stream. To transfer the grown amorphous TiO$_2$ nanotubes into a crystalline structure annealing at 350 °C and 450 °C was carried out in a tube furnace in air. After annealing, the tubes were removed from the Ti foil by sonfication in DI water.

The nanotubes were then transferred on the top of a SiN$_x$/SiO$_2$ substrate by a printing method, which means to press a TiO$_2$ bundle between the two above mentioned substrates. After this step, the substrate is blown gently with air to remove big pieces and dirt, followed by an identification of suitable nanotubes. For this, we examined the nanotubes in a Dual Beam Microscope (FEI NanoLab XT 200) and selected a particular one, see example in Fig. 1(a). To fix the nanotube on the substrate, we used electron beam induced deposition (EBID),[20] a technique based on decomposing gaseous molecules by electron beam, leading to deposition of non-volatile fragments of a given material, in our case WC$_x$. Using the electron beam, instead of the ion beam induced deposition (IBID) usually with Ga$^+$ ions, we preserve the sample structure and intrinsic characteristics. The WC$_x$ material deposited on four different places along the nanotube length, see Fig. 1(b), is nearly insulating[21] and helps to fix the sample on the substrate and also facilitates the preparation of the electrical contacts at different positions along the sample, see Fig. 1(c). To do the electrical contacts, the substrate is covered with a resist (PMMA 950 K, AR-P 671-05) for the electron beam lithography process. After developing the electrode shapes, Cr/Au thin bilayer films of thickness of 5 nm and 35 nm, respectively, were deposited by sputtering on the sample/PMMA/substrate arrangement. In the last step and after removing the rest of the PMMA, the sample is contacted to a chip carrier for the transport measurements.
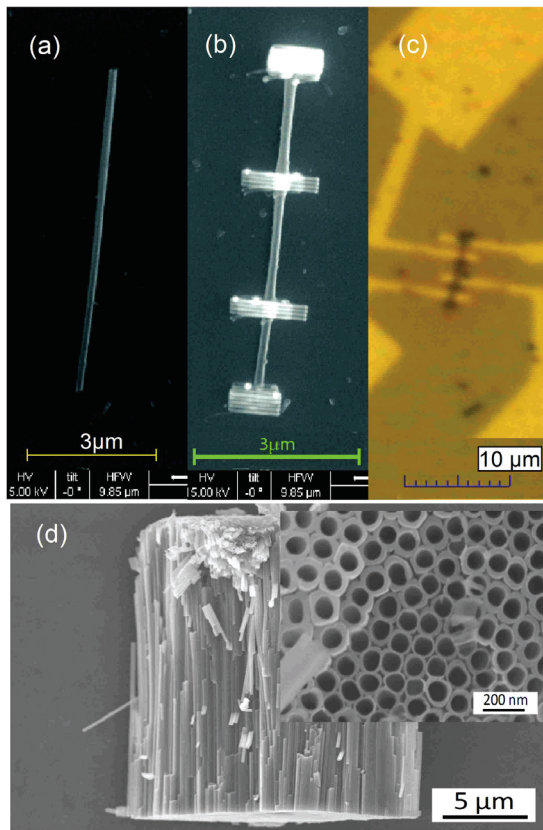
FIG. 1. (a) One TiO$_2$ nanotube before fixing it on the substrate. (b) The nanotube fixed with WC$_x$. (c) After producing the electrical contacts. (d) Scanning electron microscope side and top views (inset) of a bundle of TiO$_2$ nanotubes.

FIG. 2. Current-voltage (*I–V*) curves at different temperatures for sample TiO2a measured with four contacts. Insert: Logarithm of the normalized resistance vs. $T^{-1/4}$ for sample TiO2a at two currents, 100 nA and 500 nA. The observed linearity in the used scale indicates a 3D variable range hopping mechanism.

The carrier is mounted on the cold head of a standard closed cycle refrigerator inside a vacuum bell, with a minimal $T \simeq 25$ K. The resistance measurements were performed using a current source (Keithley 6221) and a nanovoltmeter (Keithley 2182). Impedance measurements were carried out using an Agilent 4294A impedance analyzer, in the frequency range of 40 Hz to 1 MHz at room temperature and in darkness to avoid changes due to the photoconductivity of the sample. We measured the resistance and reactance using alternating signals of 20 mV amplitude. The measurements were done in two-contacts mode, taking the two outer electrodes used for the DC resistance measurements with the sample in the same chip-carrier. The necessary calibration of the equipment to avoid spurious cables and sample holder contribution was done prior to the measurements and without the sample. Table I describes the studied samples, their length, resistance at 300 K, and the annealing treatment.

First, we discuss the results obtained using the conventional four point measurements in order to avoid possible contribu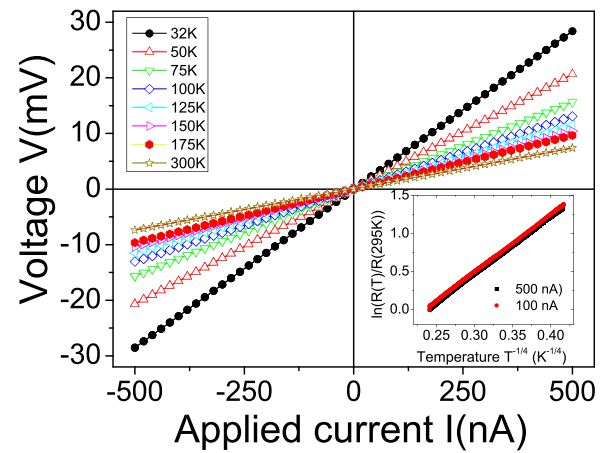tions from the contact barriers between the electrodes and the oxide surface. In this contact configuration, we observe that the *I–V* curves are linear over all the temperature range, see Fig. 2. The *T*-dependence of the resistance $R(T)$, shown in the inset of Fig. 2, indicates that

$$R(T) = R_0 \exp\left[\left(\frac{T_0}{T}\right)^{0.25}\right],$$ with R_0 an arbitrary prefactor and

T_0 a characteristic temperature coefficient. This dependence is compatible with the three dimensional (3D) variable range hopping (VRH) conduction mechanism known as the Mott law, a model that describes conduction in strongly disordered systems with localized charge-carrier states.[22] According to this model, $T_0 = 18/k_B\xi^3 N(E_F)$, where ξ is the localization length, $N(E_F)$ is the density of states at the Fermi level E_F, and k_B the Boltzmann constant. From the observed dependence, see inset in Fig. 2, we obtain $T_0 \simeq 3250$ K. Assuming that the localization length is of the order of ≈ 1 nm,[23] we estimate $N(E_F) \simeq 6.4 \times 10^{28}$ ev^{-1}m^{-3}, a value comparable with those from literature.[24]

Figure 3 shows the results of the impedance spectroscopy measurements of sample TiO2a at room temperature. Similar results were obtained for other samples. In general, for a semiconductor, different resistances and capacitances (R,C) due mainly to grain boundaries (R_{gb}, C_{gb}) and grain interior (R_g, C_g) are assumed. Each conduction process is modeled by a parallel R/C equivalent circuit. Such contributions can be in parallel or in series.[25] The process-related contributions can be recognized through a cole-cole plot by two different arcs related to the grain boundary, at low frequencies, and grain interior at higher frequencies. In the present case, see Fig. 3(a), a single arc is observed, which can be fitted with the following equation:

TABLE I. Specifications of the investigated nanotubes. The shown lengths were measured between the voltage electrodes using scanning electron microscopy. Resistivity values range between 10^{-3} and 1 Ωcm.

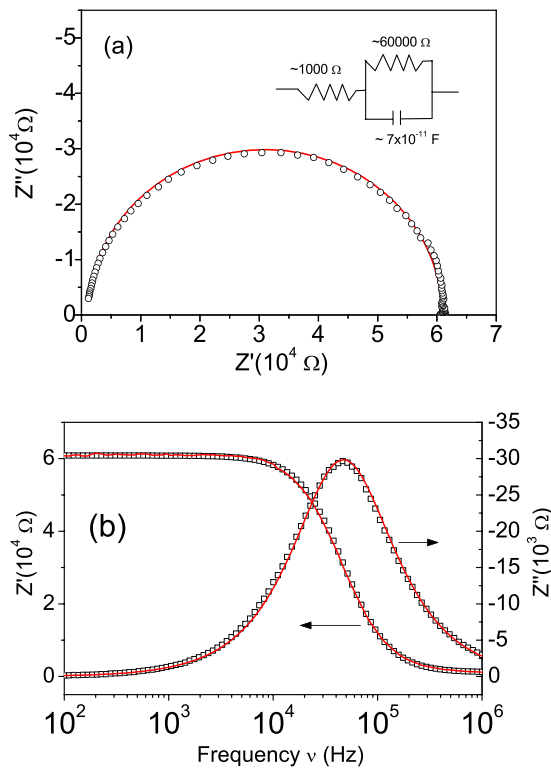|	TiO1a	TiO1b	TiO2a	TiO2b	TiO2c	TiO3b
Length (μm)	1.5 ± 0.1	1.4 ± 0.1	0.8 ± 0.1	0.5 ± 0.1	1.5 ± 0.1	0.8 ± 0.1
Annealed(1 h,air)	350 °C	350 °C	450 °C	450 °C	450 °C	450 °C
R_{300K} (kΩ)	101.3 ± 0.1	27330 ± 200	14.7 ± 0.1	11.1 ± 0.1	116.7 ± 0.1	160 ± 1

FIG. 3. (a) Nyquist plot of a single TiO_2 of sample TiO2a. The red line is the fitting to the experimental data following Eq. (1) assuming the equivalent circuit shown in the inset. (b) Frequency dependence of Z' and Z'' with their corresponding fitting curves.

$$Z^\star = Z' + iZ'' = R_0 + \left(\frac{1}{R_{g,gb}} + i\omega C_{g,gb}\right)^{-1}, \qquad (1)$$

where R_0 is the total resistance due to external component as wiring, $R_{g,gb}$ is the grain or grain boundary resistance, and $C_{g,gb}$ is the grain or grain boundary capacitance. From the fit of the data to Eq. (1), we obtained $R_0 = (10^3 \pm 50)\Omega$, $R_g = (6\pm02) \times 10^4\,\Omega$, $C_g = (7 \pm 1) \times 10^{-11}$F. The value of the capacitance indicates a conduction process through the grain cores,[26,27] in agreement with recently reported measurements in pellets of TiO$_2$ nanotubes.[28]

Furthermore and for completeness, Fig. 3(b) shows the frequency dependence of Z' and Z'' of the studied sample. The observed behavior can be well fitted with the same equivalent circuit, as expected. It can be seen that there is a single mechanism of conduction since it is possible to see a single change of slope and a single minimum for the frequency dependence of Z' and Z''.

Note that the resistances measured in all the samples indicate resistivity values below ~1 Ωcm at room temperature. These values are much smaller than the intrinsic resistivity of TiO$_2$, very probably due to the large density of intragrain defects such as oxygen vacancies, known to influence the electrical properties of this oxide.[28] These defects can facilitate the conduction within the grain, in spite of the existence of grain boundaries that do not have an appreciable contribution in the conduction process in our polycrystalline samples at room temperature.

As mentioned in the experimental section, the contacts were done by sputtering of chromium and gold. When chromium is sputtered on TiO$_2$, an oxide is formed[29] on the TiO$_2$

surface such that an extra potential barrier is formed. Each of the nanotubes has been measured using the two-point method. An example can be seen for the TiO3b sample in Fig. 4. We get a clear linear ohmic behavior at room temperature whereas at temperatures below ~150 K the contribution of an energy barrier is obvious and it becomes larger decreasing temperature. All other samples show similar I–V curves, a fact that speaks for the general formation of a potential barrier and the inadequacy of the two points method to obtain the intrinsic transport properties of several oxides. The observed behavior in the I–V curves can be understood taking into account the existence of a potential barrier and thermally activated process and the contribution of a temperature dependent ohmic term, given by the equation

$$V = a(T)\tanh(I/I_0) + b(T)I, \qquad (2)$$

where $a(T)$, $b(T)$, and I_0 are fitting parameters. In Fig. 4, we show the fits of the I–V curves following Eq. (2). From these fits, we obtain that $a(T) \simeq 26[VK]/T$, $I_0 \simeq 1\,\mu A$, and $b(30K) \simeq 4.6 \times 10^5\,\Omega$, decreasing slightly with T.

The results of the temperature dependence of the resistance at different constant currents are shown in the inset of Fig. 4. At low input currents, the normalized resistance follows roughly an inverse temperature dependence due to the influence of the potential barrier, which is the reason for the non-linear I–V characteristics shown in Fig. 4. Obviously, this influence decreases with temperature and current; it remains negligible at $T > 150$ K, temperature range where the resistance shows an ohmic behavior.

Concluding, we have isolated TiO$_2$ nanotubes within the micro- and nanometer scale and we were able to contact them using a combination between electron beam induced deposition and electron beam lithography for electronic transport measurements. The temperature dependent of the resistance is described by the Mott variable range hopping mechanism. The usage of Cr/Au contacts for transport measurement at temperatures below 150 K does produce a measurable potential barrier. Impedance spectroscopy results
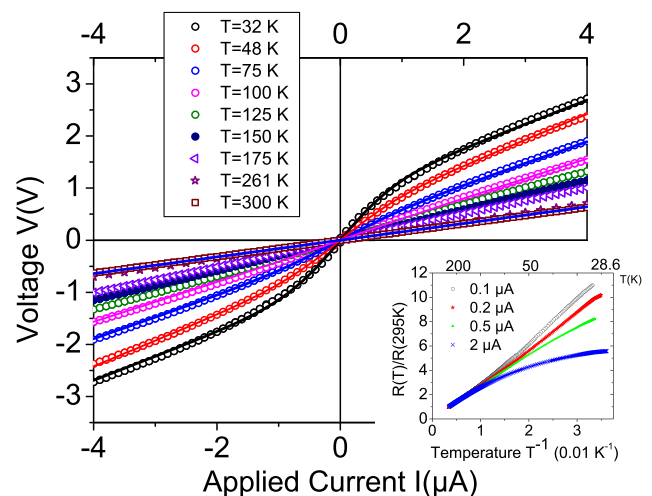

FIG. 4. Current-voltage characteristics for sample TiO3b. The continuous lines through the points at five different temperatures (32 K, 48 K, 75 K, 100 K, and 300 K) follow Eq. (2). Inset: Normalized resistance vs. inverse temperature for sample TiO3b at different constant currents.

indicate that a single transport through the grain cores is active.

[1] K. I. Hadjiivanov and D. G. Klissurski, Chem. Soc. Rev. **25**, 61 (1996).

[2] A. Fujishima and K. Honda, Nature **238**, 37 (1972).

[3] B. O'Regan and M. Grätzel, Nature **353**, 737 (1991).

[4] M.-H. Seo, M. Yuasa, T. Kida, J.-S. Huh, K. Shimanoe, and N. Yamazoe, Sens. Actuators B **137**, 513 (2009).

[5] A. S. Aricò, P. Bruce, B. Scrosati, J. Tarascon, and W. van Schalkwijk, Nat. Mater. **4**, 366 (2005).

[6] U. Diebold, Surf. Sci. Rep. **48**, 53 (2003).

[7] X. Chen and S. S. Mao, Chem. Rev. **107**, 2891 (2007).

[8] H. Tang, K. Prasad, R. Sanjinbs, P. E. Schmid, and F. Levy, J. Appl. Phys. **75**, 2042 (1994).

[9] L. Forro, O. Chauvet, D. Emin, L. Zuppiroli, H. Berger, and F. Levy, J. Appl. Phys. **75**, 633 (1994).

[10] J. M. Macak, M. Zlamal, J. Krysa, and P. Schmuki, Small **3**, 300 (2007).

[11] X. Liu, P. K. Chu, and C. Ding, Mater. Sci. Eng. R **47**, 49 (2004).

[12] P. Roy, S. Berger, and P. Schmuki, Angew. Chem. Int. Ed. **50**, 2904 (2011).

[13] A. G. Muñoz, Electrochem. Acta **52**, 4167 (2007).

[14] S. P. Albu, H. Tsuchiya, S. Fujimoto, and P. Schmuki, EJIC **2010**, 4351 (2010).

[15] A. W. Czanderna, C. N. R. Rao, and J. M. Honig, Trans. Faraday Soc. **54**, 1069 (1958).

[16] H. Mirabolghasemi, N. Liu, K. Lee, and P. Schmuki, Chem. Comm. **49**, 2067 (2013).

[17] S. P. Albu, A. Ghicov, S. Aldabergenova, P. Drechsel, D. LeClere, G. E. Thompson, J. M. Macak, and P. Schmuki, Adv. Mater. **20**, 4135 (2008).

[18] J. R. Macdonald and J. A. Garber, J. Electrochem. Soc. **124**, 1022 (1977).

[19] M. Hattori, K. Noda, T. Nishi, K. Kobayashi, H. Yamada, and K. Matsushige, Appl. Phys. Lett. **102**, 043105 (2013).

[20] M. Huth, F. Porrati, C. Schwalb, M. Winhold, R. Sachser, M. Dukic, J. Adams, and G. Fantner, Beilstein J. Nanotechnol. **3**, 597 (2012).

[21] D. Spoddig, K. Schindler, P. Rödiger, J. Barzola-Quiquia, K. Fritsch, H. Mulders, and P. Esquinazi, Nanotechnology **18**, 495202 (2007).

[22] N. F. Mott, J. Non-Cryst. Solids **1**, 1 (1968).

[23] L. X. Chen, T. Rajh, Z. Wang, and M. C. Thurnauer, J. Phys. Chem. B **101**, 10688 (1997).

[24] A. Yildiz, S. B. Lisesivdin, M. Kasap, and D. Mardare, Optoelectron. Adv. Mater.-Rapid Commun. **1**, 531 (2007).

[25] S. M. Haile, D. L. West, and J. Campbell, J. Mater. Res. **13**, 1576 (1998).

[26] *Impedance Spectroscopy: Theory, Experiment, and Applications*, edited by E. Barsoukov and J. R. MacDonald (John Wiley & Sons Inc., New York, 2005).

[27] E. Chinarro, J. R. Jurado, F. M. Figueiredo, and J. Frade, Solid State Ionics **160**, 161 (2003).

[28] P. P. Vijayan, M. Thomas, and K. C. George, J. Appl. Phys. **112**, 104308 (2012).

[29] C. Winde, *Herstellung und Charakterisierung von Cr-Schichten auf TiO$_2$-(110) Oberflächen* (Max-Planck-Institut für Metallforschung, Stuttgart, 2002).